View metadata, citation and similar papers at core.ac.uk

brought to you by CORE

provided by Boise State University - ScholarWorks

Boise State University
ScholarWorks

Geosciences Faculty Publications and Presentations | Department of Geosciences

2-1-2014

Application of a Hillslope-Scale Soil Moisture Data Assimilation System to Military Trafficability Assessment

Alejandro N. Flores
Boise State University

Dara Entekhabi
Massachusetts Institute of Technology

Rafael L. Bras
Georgia Institute of Technology

NOTICE: this is the author's version of a work that was accepted for publication in *Journal of Terramechanics*. Changes resulting from the publishing process, such as peer review, editing, corrections, structural formatting, and other quality control mechanisms may not be reflected in this document. Changes may have been made to this work since it was submitted for publication. A definitive version was subsequently published in *Journal of Terramechanics*, Vol. 51, (2014). DOI: 10.1016/j.jterra.2013.11.004

NOTICE: This is the author's version of a work that was accepted for publication in *Journal of Terramechanics*. Changes resulting from the publishing process, such as peer review, editing, corrections, structural formatting, and other quality control mechanisms may not be reflected in this document. Changes may have been made to this work since it was submitted for publication. A definitive version was subsequently published in *Journal of Terramechanics*, Vol. 51, (2014). DOI: 10.1016/j.jterra.2013.11.004

Application of a Hillslope-Scale Soil Moisture Data Assimilation System to Military Trafficability Assessment

Alejandro N. Flores
Lead and corresponding author
Assistant Professor
Department of Geosciences
Boise State University
Email: lejoflores@boisestate.edu

Dara Entekhabi
Bacardi and Stockholm Water Foundations Professor
Department of Civil and Environmental Engineering, and
Department of Earth, Atmospheric and Planetary Sciences
Massachusetts Institute of Technology

Rafael L. Bras
Departments of Civil and Environmental Engineering and Earth, and
Atmospheric Sciences Georgia Institute of Technology

ABSTRACT

Soil moisture is an important environmental variable that impacts military operations and weapons systems. Accurate and timely forecasts of soil moisture at appropriate spatial scales, therefore, are important for mission planning. We present an application of a \ soil moisture data assimilation system to military trafficability assessment. The data assimilation system combines hillslope-scale (e.g., 10s to 100s of m) estimates of soil moisture from a hydrologic model with synthetic L-band microwave radar observations broadly consistent with the planned NASA Soil Moisture Active-Passive (SMAP) mission. Soil moisture outputs from the data assimilation system are input to a simple index-based model for vehicle trafficability. Since the data assimilation system uses the ensemble Kalman Filter, the risks of impaired trafficability due to uncertainties in the observations and model inputs can be quantified. Assimilating the remote sensing observations leads to significantly different predictions of trafficability conditions and associated risk of impaired trafficability, compared to an approach that propagates forward uncertainties in model inputs without assimilation. Specifically, assimilating the observations is associated with an increase in the risk of "slow go" conditions in approximately two-thirds of the watershed, and an increase in the risk of "no go" conditions in approximately 40% of the watershed. Despite the simplicity of the trafficability assessment tool, results suggest that ensemble-based data assimilation can potentially improve trafficability assessment by constraining predictions to observations and facilitating quantitative assessment of the risk of impaired trafficability.

Highlights:
1. We apply a soil moisture data assimilation system (DAS) to military trafficability
2. Assimilation improves prediction of impaired trafficability
3. Ensemble-based assimilation supports quantification of trafficability risk

Keywords: Soil moisture; military trafficability; data assimilation; remote sensing, microwave radar; hillslope scale

NOTICE: This is the author's version of a work that was accepted for publication in *Journal of Terramechanics*. Changes resulting from the publishing process, such as peer review, editing, corrections, structural formatting, and other quality control mechanisms may not be reflected in this document. Changes may have been made to this work since it was submitted for publication. A definitive version was subsequently published in *Journal of Terramechanics*, Vol. 51, (2014). DOI: 10.1016/j.jterra.2013.11.004

1. Introduction

The purpose of this study is to demonstrate how forthcoming satellite radar observations that are sensitive to soil moisture can potentially be used to improve assessment of military vehicle trafficability by combining those observations with information from a hydrologic model. Estimation of the spatiotemporal distribution of soil moisture is critical for weather, climate, and hydrologic forecasting [1]. As a military battle-space environment variable, moreover, soil moisture exerts considerable influence on mobility and trafficability [2]. At scales of individual hillslopes (10s to 100s of m), for instance, soil wetness can limit mobility of military vehicles and personnel over the land surface, thereby potentially impacting mission outcomes and decision-making. Because of the importance of soil moisture on mission planning and execution, improving the accuracy, timeliness, and spatial resolution of soil moisture can enhance military decision support systems.

An increasingly important methodology for estimating soil moisture is data assimilation – the mathematical combination of model- and observation-based soil moisture information [3, 4]. Advantages of data assimilation as a soil moisture estimation technique include the ability to: (1) use observations and models of different spatial resolutions [5], (2) ingest observations of geophysical variables that are indirectly related to soil moisture [6-8], and (3) constrain model soil moisture predictions to observations that are intermittently available [9]. Ensemble-based techniques, such as the ensemble Kalman Filter (EnKF) [10, 11] and Markov Chain Monte Carlo [12] methods, are a particular class of data assimilation methods that support the use of Monte Carlo simulation to resolve the spatiotemporal distribution of soil moisture in a probabilistic way. Other techniques, known as smoothers [13], can use observations to update model estimates at all times. For the sake of simplicity, we limit our discussion to the introduction of data assimilation techniques based on the EnKF. Readers interested in a broader review of data assimilation techniques should refer to reviews by [14].

In the EnKF framework, uncertainties in boundary (e.g., soil properties, rainfall forcing) and initial (e.g., soil moisture) conditions are represented explicitly by producing stochastic realizations of model states (e.g., soil moisture and temperature), parameters (e.g., soil and vegetation parameters) and forcings (e.g., precipitation and humidity). Stochastic realizations of initial and boundary conditions are then propagated through the hydrologic forecasting model. The output is an ensemble of soil moisture realizations (referred to as the *forecast*) from which the sample mean, variance, and covariance are computed. These sample statistics are assumed to approximate the underlying spatial probability density function of soil moisture. The ensemble of model soil moisture estimates is conditioned on observations that are also associated with uncertainty, expressed as an error covariance matrix. The conditioned ensemble of model soil moisture estimates (referred to as the *analysis*) is an initial condition to the hydrologic model, which is evolved forward in time (under still-uncertain boundary conditions) until a new observation is available. This forecast-analysis process repeats for every subsequent observation.

We use the outputs of a soil moisture data assimilation system as input to a simple model of vehicle mobility. The vehicle mobility model is based on the concept of the Rating Cone Index (RCI) [15,16], a measure of soil surface load-bearing capacity, and a Vehicle Cone Index (VCI) [16,17], vehicle-specific critical values of RCI that are indicative of impaired mobility. The soil moisture data assimilation system, described in detail by Flores et al. [2012], uses a physics-based ecohydrology model (described below) to simulate the spatiotemporal distribution of soil moisture at the hillslope scale. Uncertainty in boundary conditions is represented in: (1) soil parameters using a Latin-hypercube based sampling strategy (see [18]), and (2) hydrometeorologic forcings using a stochastic weather generator (see [8,19]). Observations used to condition soil moisture ensembles take the form of synthetic L-band microwave radar images broadly consistent with NASA's forthcoming Soil Moisture Active-Passive (SMAP) satellite [20]. Because this satellite is not yet in orbit, we use an Observing System Synthetic Experiment (OSSE) approach in which the ecohydrologic model is used to simulation a notionally true realization of the spatiotemporal distribution of soil moisture. Output from the ecohydrology model is supplied as input to the Integral Equation Model [7,21-23]] to yield synthesized images of radar backscatter in two polarization states (see [8]). Because topography is correlated with factors affecting reflection of microwave energy like soil moisture (e.g., [24]) and controls the local incidence and polarization, the observation synthesis approach explicitly accounts for topography (e.g., [25,26]).

NOTICE: This is the author's version of a work that was accepted for publication in *Journal of Terramechanics*. Changes resulting from the publishing process, such as peer review, editing, corrections, structural formatting, and other quality control mechanisms may not be reflected in this document. Changes may have been made to this work since it was submitted for publication. A definitive version was subsequently published in *Journal of Terramechanics*, Vol. 51, (2014). DOI: 10.1016/j.jterra.2013.11.004

We seek to address the following applied science questions:

(1) Do improvements in the accuracy of soil moisture knowledge correspondingly improve the accuracy of trafficability maps?

(2) For a given vehicle, does constraining model-derived soil moisture to satellite observations significantly change the perceived risk of impaired trafficability conditions?

In section 2 below we describe the study methods. This includes a brief overview of the data assimilation system used to obtain soil moisture ensembles used for trafficability assessment and the trafficability assessment technique. Section 3 presents the results of the simulation experiments. Key findings, implications, and potential directions for future study are discussed in Section 4.

2. Methods

The SMAP satellite is not scheduled for launch until late 2014 and there is currently no L-band radar satellite that provides adequate spatial resolution and temporal revisit to support military trafficability assessment using the data assimilation approach described here. An OSSE approach is therefore required. The OSSE framework is commonly used in geophysical inversion, remote sensing, and data assimilation studies to develop inversion algorithms and test the accuracy of data assimilation routines prior to the availability of actual observations [6-8]. In an OSSE framework, a model of the physical system is used to produce a synthetic (i.e., hypothetical) distribution of soil moisture that is conceptually "true." A geophysical forward model is then used to create a corresponding set of synthetic observations of the variable that is observed by the sensor (i.e., brightness temperature for passive microwave, or radar backscatter or travel time for radar). Synthetic observations are then perturbed with noise that is consistent with the anticipated observational error to produce synthetic satellite products that are used in a data assimilation experiment (i.e., with the EnKF algorithm). Outputs of the data assimilation experiment – estimates of the distribution of soil moisture and a measure of uncertainty – are then compared with the model-derived true soil moisture distribution. Typically, a corresponding ensemble simulation – without assimilation performed – is also conducted to quantify uncertainties in soil moisture in the absence of constraint on observational data. This is referred to as an open loop (OL) simulation. The relative estimation errors of the data assimilation and open loop simulations reveal the extent to which ingesting observational data improves predictions in soil moisture, assuming that the model and observations are not biased with respect to each other.

This section details the development of the hillslope-scale data assimilation system and how it is applied to produce trafficability maps.

2.1 Hillslope-scale research data assimilation system

This subsection provides an overview of the data assimilation system used to derive soil moisture ensembles that are subsequently used to perform a simple trafficability analysis. The core components of this research data assimilation system are the: (1) ecohydrologic model, (2) satellite observations, (3) data assimilation algorithm, and (4) experimental conditions and assumptions. A conceptual workflow of this data assimilation-based trafficability assessment tool is shown in Figure 1.

2.1.1 Hillslope-scale soil moisture modeling

The simulation core of the hillslope-scale data assimilation system is a coupled biophysical and hydrologic system referred to as the Triangulated Irregular Network (TIN)-based Realtime Integrated Basin Simulator (tRIBS) [27,28] and VEGetation Integrated Evolution (VEGGIE) [29,30] models (collectively tRIBS-VEGGIE). The tRIBS-VEGGIE resolves mass, energy and carbon balance at hillslope scales (10s to 100s of m) within a watershed. Watershed topography is represented with a TIN and associated Voronoi polygon map obtained an underlying digital elevation model (DEM) (e.g., [31]). The TIN representation leads to a variable spatial resolution within a watershed, reducing computational demands of model simulations while preserving the distribution of slope, aspect, and other key attributes of topography. A full description of the tRIBS-VEGGIE model is outside the scope of this applied study. The reader is referred to [27-30] for a more extensive overview of the model physics and [8,18,26] for its application in the development of the data assimilation framework used in this study.

NOTICE: This is the author's version of a work that was accepted for publication in *Journal of Terramechanics*. Changes resulting from the publishing process, such as peer review, editing, corrections, structural formatting, and other quality control mechanisms may not be reflected in this document. Changes may have been made to this work since it was submitted for publication. A definitive version was subsequently published in *Journal of Terramechanics*, Vol. 51, (2014). DOI: 10.1016/j.jterra.2013.11.004

Inputs to the tRIBS-VEGGIE model include hourly hydrometeorological forcings, soil hydraulic and thermal properties, vegetation parameters, and a static elevation field representing watershed topography. Hydrometeorological forcings to the model include hourly precipitation, sky fractional cover or incoming solar radiation, air temperature, dew temperature, and wind speed.

2.1.1 Synthetic L-band microwave radar observations

Because the soil dielectric in the microwave region of the electromagnetic spectrum is sensitive to the degree of saturation [32], microwave remote sensing has become a critical tool for global soil moisture observation. The L-band (1-2 GHz) of the microwave region is particularly advantageous for soil moisture observation because in this region the atmosphere is essentially transparent and microwave penetration into the soil is deeper than at higher frequencies [20,33,34]. As a result, two satellite platforms (one operational, one planned) utilize L-band microwave technology to measure soil moisture globally approximately every 2-3 days. The European Space Agency's Soil Moisture and Ocean Salinity (SMOS) mission, operational since late 2009, uses a microwave radiometer to retrieve soil moisture at spatial resolutions of approximately 50 km [33,34]. The NASA Soil Moisture Active-Passive (SMAP) satellite, scheduled to launch in late 2014 [20], will co-locate an L-band microwave radiometer with a frequency of 1.41 GHz (spatial resolution ~40 km) and a synthetic aperture radar with a frequency of 1.26 GHz (spatial resolution ~1-3 km). A combined active-passive soil moisture product will achieve a global spatial resolution of approximately 10 km. Despite the timely nature of the 2-3 day revisit period of these satellites, the resolution of the associated data products is nevertheless too coarse for direct insertion into trafficability assessment tools requiring information at hillslope scales.

These coarse-scale observations can still be used in a data assimilation framework to improve estimates of soil moisture at hillslope scales derived from the tRIBS-VEGGIE model. Assimilation systems can be formulated such that either the retrieved (e.g., soil moisture) or geophysically observed (e.g., backscatter or radiance) quantity is used to update the model. In the case of the data assimilation system used here, L-band radar backscatter observations at 3 km spatial resolution and two polarization states (*hh* and *vv*) are assimilated directly. This approach necessitates a forward model to predict the observed quantity (radar backscatter) given the soil moisture estimate from tRIBS-VEGGIE. Soil moisture maps derived from tRIBS-VEGGIE are used to derive corresponding maps of the soil dielectric constant using the Topp model [32]. Based on the local topographic slope and aspect maps, local incidence and polarization rotation angles are computed [25,26], and together with the derived dielectric constant, soil reflectivity maps in horizontal and vertical co-polarized states are determined through the Fresnel equations [7,21-23]. The Integral Equation Model (IEM) is then used to compute the spatial maps of radar backscatter in *hh*- and *vv*-polarization, assuming known roughness characteristics of the soil. Hillslope-scale maps of radar backscatter on the tRIBS-VEGGIE TIN mesh are then averaged to a 3 km square grid (consistent with the SMAP level 1 radar product, see [20]). A thorough overview of this forward model is presented in Flores et al. [8,26].

2.1.3 Data assimilation algorithm

The ensemble Kalman Filter (EnKF) is a sequential data assimilation algorithm and a Monte-Carlo simulation-based generalization of the Kalman Filter [10,11,35]. A key strength of the EnKF is that, because the state error covariance is estimated from an ensemble of Monte Carlo simulations, it does not require the use of a model with linear or linearized dynamics. Additionally, because the update involves only stopping and starting an ensemble of simulations, the observations being assimilated can be temporally intermittent. On the other hand, because the model state update is based only on first- and second-order statistics, it assumes that the state and observational errors are Gaussian and white. A full review of the EnKF is beyond the scope of this paper. The particular EnKF algorithm used in the data assimilation system is outlined in [11].

NOTICE: This is the author's version of a work that was accepted for publication in *Journal of Terramechanics*. Changes resulting from the publishing process, such as peer review, editing, corrections, structural formatting, and other quality control mechanisms may not be reflected in this document. Changes may have been made to this work since it was submitted for publication. A definitive version was subsequently published in *Journal of Terramechanics*, Vol. 51, (2014). DOI: 10.1016/j.jterra.2013.11.004

In the context of this work, the following represent the key sequential steps in the EnKF framework to update hillslope-scale estimates of soil moisture from tRIBS-VEGGIE with L-band microwave radar observations:

1. The tRIBS-VEGGIE model is initialized with an initial ensemble of soil moisture realizations.

2. Each realization of the initial soil moisture ensemble is propagated forward in time using the tRIBS-VEGGIE model, subject to a corresponding realization of boundary conditions (hydrometeorological forcings) and soil parameters. This yields a forecast ensemble at the time of L-band radar observation.
3. Using the forward model, each realization of the forecast ensemble is used to produce a corresponding prediction of the microwave radar observation. This produces an ensemble forecast of the 3 km L-band radar observations.

4. The sample cross-covariance matrix between the forecast soil moisture ensemble and forecast observation ensemble is computed.

5. With the actual 3 km L-band radar observation, and an assumed or deduced error covariance matrix associated with the observations, the Kalman gain matrix is computed.

6. The Kalman gain matrix is multiplied by the innovations, the difference between the forecast and actual L-band radar observation, and the product added to the forecast soil moisture ensemble. This matrix is the analysis soil moisture ensemble; individual soil moisture realizations that have been conditioned on the observation.

7. The soil moisture realizations within the analysis ensemble are used to re-initialize the tRIBS-VEGGIE model, and steps 2-6 repeated for subsequent observations.

A conceptual diagram of the EnKF algorithm is shown in Figure 2.

2.1.4 Experimental Setup

The OSSE is set in the Walnut Gulch Experimental Watershed (WGEW) in Arizona, USA (area148 km^2). The semiarid watershed is associated with a mean annual temperature of 17.7 °C, while mean annual precipitation is 312 mm [36]. The distribution of elevation, topographic slope, soil textures, and total precipitation over the course of the experiment, as well as the location of the watershed, is shown in Figure 3. Vegetation cover in WGEW is dominated by desert shrubs, which cover approximately two-thirds of the watershed. The most common shrubs include creosote, tarbush, mortonia, and whitethorn. The remaining one-third of the watershed is covered by grasslands with black grama, curly mesquite grass, and tobosa grass predominating.

Hydrometeorological forcings for the OSSE were produced with a stochastic weather generation approach. Hourly precipitation was generated using the Modified Bartlett-Lewis (MBL) model (e.g., [37]) using parameters for Tucson International Airport, Arizona, USA [19]. An ensemble of precipitation realizations was produced by stochastically disaggregating hourly precipitation values to a 4 km grid using a multiplicative cascade [38]. The remainder of the hydrometeorological forcings required by tRIBS-VEGGIE (e.g., temperature, humidity, windspeed) were obtained using the stochastic weather generator summarized in [19].

The spatial organization of soil textural classes corresponding to mapped soil units is assumed known, but the soil parameters required as input to tRIBS-VEGGIE for each mapped soil unit is assumed uncertain. The spatial distribution of soil units for WGEW was obtained from the Soil Survey Geographic (SSURGO) database maintained and published by the USDA. For brevity we do not reproduce here a table of soil textures along with the map in Figure 3(e), but the reader is referred to [8] for this information. Within each soil textural unit in the map (Fig. 3(c)) an ensemble of soil parameters was generated stochastically using a Latin Hyper-cube based approach outlined in [18]. This approach produces an ensemble of parameters that preserves observe correlation among soil properties.

An additional and independent realization of soil properties and hydrometeorological forcings was propagated through tRIBS-VEGGIE to produce the synthetic true soil moisture distribution. This synthetic true simulation was 648 hours (27 days) in duration, with parameters for the MBL consistent with July. At 72-hour intervals (consistent with the SMAP mission revisit), the true soil moisture distribution was input to the forward model to yield the synthetic true L-band radar observations in horizontally and vertically co-polarized states. These synthetic true

NOTICE: This is the author's version of a work that was accepted for publication in *Journal of Terramechanics*. Changes resulting from the publishing process, such as peer review, editing, corrections, structural formatting, and other quality control mechanisms may not be reflected in this document. Changes may have been made to this work since it was submitted for publication. A definitive version was subsequently published in *Journal of Terramechanics*, Vol. 51, (2014). DOI: 10.1016/j.jterra.2013.11.004

observations were then perturbed with additive Gaussian noise that is zero mean with a standard deviation of 0.5 dB. This yields synthetic observations to be assimilated. Speckle noise common to radar images is more appropriately simulated as multiplicative noise (e.g., [39]). However, due to the small number of radar pixels required to cover the domain (7 x 10) the differences in the spatial structure of simulated noise between error models is negligible.

The EnKF experiment was performed with 256 ensemble replicates. The 648 hr experiment period corresponds to nine simulated SMAP over-flights and, therefore, nine forecast-analysis cycles. For comparative purposes, a 1024 member open loop (OL) ensemble was also simulated. In the OL simulation, uncertainties in model parameters and initial and boundary conditions are propagated through the tRIBS-VEGGIE model, without being conditioned on the synthetic radar observations. The OL represents an "uninformed" forecast of soil moisture and trafficability conditions.

The reader is referred to the work of [8] for a thorough presentation of these experiments, results, underlying assumptions, and limitations of the experimental framework. For the purposes of this trafficability assessment application, we focus on results of the third analysis cycle (AN3) at hour 216 of the experiment. This analysis occurred immediately after a large rainfall event when we would expect the influence of increased moisture on impaired trafficability to be at its maximum during the experiment. We are specifically interested in the degree to which soil moisture data assimilation with the EnKF allows for improved knowledge of soil moisture, expected trafficability, and trafficability risk compared to the OL experiment. Estimation errors in both soil moisture and a trafficability index for both the EnKF and OL experiments are computed relative to the synthetic true tRIBS-VEGGIE soil moisture and associated trafficability index at AN3. Characteristics of the synthetic experiment are summarized in Table 1.

2.2 Trafficability assessment model

Trafficability assessment is often done using field-based surveys performed by military personnel (e.g., [16, 40-42]). The US Army Corps of Engineers has developed standard in situ techniques for trafficability assessment, using a variety of devices including a handheld cone penetrometer (PCP) ([41]). The PCP measures the compressive and frictional resistance of the soil as it is forced vertically downward into the soil column. This resistance, typically reported in units of force per unit area, is referred to as the cone index (*CI*). For fine grained soils, *CI* is multiplied by a reducing index of soil remoldability (*RI*) to achieve the remold cone index (*RCI*) . The soil layer supporting the mass of the vehicle is referred to as the critical layer and varies by the soil type, soil strength profile, and the type and weight of the vehicle [42]. Consistent with [43], we assume the critical layer extends from the surface to 40 cm in depth, and use the following statistical model to predict *RCI* as a function of volumetric soil moisture,

$$RCI = \exp\left(a + b\ln\theta_{\%}\right) \tag{1}$$

where soil moisture is expressed as a percentage value $\theta_{\%}$, and regression coefficients a and b depend on the soil textural class. Values of a and b for different soil textural classes are shown in Table 2. As the values of b in Table 2 suggest, *RCI* decreases as soil moisture increases, and the relationship between *RCI* and soil moisture varies by soil texture. Ensemble soil moisture estimates from the EnKF and OL experiments are input to equation (1) to produce corresponding ensembles of *RCI*. The spatial distribution of ensemble *RCI* statistics, however, are difficult to interpret in the context of trafficability assessment without additional refining. Therefore, we investigate how the spatial variability of hillslope-scale soil moisture, through its influence on *RCI*, impacts the trafficability performance of a particular vehicle-type.

The vehicle cone index (*VCI*) is defined as a minimum value of *RCI* for fine-grained soils and *CI* for coarse-grained soils required for a particular vehicle to achieve a given number of passes over a soil [40]. The single-pass vehicle cone index (VCI_1) is a vehicle performance metric that corresponds to the value of *RCI* at which that vehicle-type would experience impaired mobility after one pass through the soil. Similarly, the fifty-pass vehicle cone index (VCI_{50}) corresponds to the value of *RCI* at which that vehicle-type would experience impaired mobility after fifty passes through the soil. VCI_1 and VCI_{50} are used together in trafficability assessment, along with other landscape metrics not considered here such as ground slope, as indicators of expected performance for a particular vehicle-type. For the purpose of this study, we refer to $VCI_1 < RCI \leq VCI_{50}$ as "slow-go'" conditions, and $RCI \leq VCI_1$ as "no-go" conditions. In this work, we investigate the expected trafficability conditions for a wheeled Light Armored Vehicle (LAV) armored personnel carrier. Values of VCI_1 and VCI_{50} for the LAV-25 are 32 and 72, respectively (see [44], Appendix D).

NOTICE: This is the author's version of a work that was accepted for publication in *Journal of Terramechanics*. Changes resulting from the publishing process, such as peer review, editing, corrections, structural formatting, and other quality control mechanisms may not be reflected in this document. Changes may have been made to this work since it was submitted for publication. A definitive version was subsequently published in *Journal of Terramechanics*, Vol. 51, (2014). DOI: 10.1016/j.jterra.2013.11.004

In this trafficability case study we are interested in: (1) the spatial distribution expected trafficability conditions, as measured by the ensemble mean of *RCI*, and (2) the risk of the vehicle encountering impaired trafficability conditions throughout the landscape. Risk of impaired trafficability conditions are diagnosed from the ensemble of *RCI* values. At a particular location in the watershed, the risk of slow-go conditions is calculated as the number of ensemble replicates exhibiting $VCI_1 < RCI \leq VCI_{50}$, relative to the ensemble size (256 for EnKF, 1024 for OL). Similarly, the risk of no-go conditions is calculated as the number of ensemble replicates exhibiting $RCI \leq VCI_1$, relative to ensemble size.

It should be noted that the trafficability model presented here assumes that soil moisture is the only landscape factor limiting mobility of the hypothetical LAV. This is an oversimplification of the multi-factorial and potentially interacting terrain variables (e.g., slope gradient, land cover) that potentially limit vehicle mobility that may overemphasize the importance of soil moisture. For instance, in areas of slope steepness that exceed a maximum slope that limits trafficability of a particular vehicle, the soil moisture/strength is irrelevant. Hence, the trafficability assessments presented here are not meant to reflect an all-encompassing tactical decision aid that might be used in application. Although simplistic, this approach does allow us to examine the extent to which assimilation of remotely sensed information into a model can improve the component of trafficability knowledge that is related to soil moisture in isolation of these other, potentially confounding, variables.

3. Results

The results of the EnKF and OL simulations used to perform the trafficability assessment presented in this work are a subset of the larger set of experiments conducted and described in [8]. For brevity, we present results of those experiments related to soil moisture only insofar as they assist in interpreting the results of the trafficability assessment. Those readers interested in a more detailed discussion of the impact of data assimilation on soil moisture estimates are referred to that previous work. For comparative purposes, the distribution of soil moisture associated with the true soil moisture is shown in Figure 4(a). Ensemble mean soil moisture in the top 40 cm of the soil profile is substantially different between the EnKF and OL experiments (Figs. 4(b) and 4(c)). The spatial distribution of the ensemble mean soil moisture of the OL simulation reflects the influence of spatial heterogeneity in soil texture and topography (Fig. 4(b)). Heterogeneity in soil texture and topography on the spatial distribution of soil moisture is also apparent in the EnKF ensemble mean, but exhibits vertical and horizontal linear features visible in the central part of the watershed (Fig. 4(c)). These linear features are coincident with the grid cells of the rainfall forcings, indicating that assimilation of the radar observations somewhat compensates for uncertainty in rainfall. This is significant because AN3 (analysis cycle 3) closely follows a significant rainfall event. The spatial distribution of soil textural classes can also clearly be seen and are often are associated with relatively large spatial gradients in the ensemble mean soil moisture while channels and valley networks are often visible within a particular soil type (Fig. 4(c)). Assimilation of the observations decreases the estimation error throughout the vast majority of the watershed, depicted as the root mean squared error (RMSE) in soil moisture in the top 40 cm of the soil column relative to the open loop ensemble (Figs. 4(d) and 4(e)). At each pixel within the watershed, RMSE is reduced by an average of 36% due to assimilation (Table 3). However, some of the larger channel and valley network features, which are associated with substantially wetter conditions (Fig. 4(c)), still exhibit large estimation errors after assimilation (Fig. 4(e)). Table 3 summarizes the watershed averaged ensemble mean soil moisture and RMSE in soil moisture for the OL and EnKF experiments. Lack of a substantial reduction in estimation errors after assimilation in these regions suggests that they: (1) do not occupy sufficient area to substantially influence the predicted 3 km-scale radar observations, and/or (2) are associated with locally unique soil and topographic conditions that are not sufficiently correlated with the predicted radar observations during the update.

Despite relatively wet conditions, the majority of the watershed is associated with relatively high values of *RCI*, indicating relatively strong local soil conditions (Figs 5(a)-(c)). Assimilation of the synthetic observations, however, results in substantial differences in the ensemble mean *RCI* between the EnKF and OL experiments. Specifically, assimilation leads to some soil types (particularly in the South-central and central portions of the watershed) that exhibit substantially lower values of *RCI* than in the OL case (Figs. 5(b) and 5(c)). Hence, in areas where the EnKF results in more moisture than the OL case, assimilation has the potential to reveal trafficability conditions that are worse than the OL estimate would suggest. Assimilation also leads to a substantially lower RMSE in *RCI* throughout much, though not all, of the watershed (Figs. 5(d) and 5(e)).

NOTICE: This is the author's version of a work that was accepted for publication in *Journal of Terramechanics*. Changes resulting from the publishing process, such as peer review, editing, corrections, structural formatting, and other quality control mechanisms may not be reflected in this document. Changes may have been made to this work since it was submitted for publication. A definitive version was subsequently published in *Journal of Terramechanics*, Vol. 51, (2014). DOI: 10.1016/j.jterra.2013.11.004

Data assimilation has a fairly dramatic impact on the diagnosed trafficability risk. The EnKF estimate of trafficability risk is associated with substantially higher frequency of slow-go conditions in several soil units (Figs. 6(a) and 6(b)). In some soil units in the southwestern portion of the watershed, for instance, the probability of encountering slow-go conditions is relatively low (< 33% chance) for the OL experiment, but high (> 66% chance) for the EnKF experiment (Figs. 6(a) and 6(b)). While the spatial organization of soil units explains much of the differences in trafficability risk, some finer scale effects, related to topography, are seen in the south-central part of the watershed (Fig. 6(b)). There are also dramatic differences in the risk of no-go trafficability conditions between the EnKF and OL experiments (Figs. 6(c) and 6(d)). Some soil units in the south-central part of the watershed exhibit a low probability (0.00-0.20) of no-go conditions in the OL experiment (Fig. 6(c)), yet exhibit very high probability (0.80-1.00) of no-go conditions in the EnKF experiment (Figs. 6(d)). The EnKF experiment suggests a slightly higher risk of no-go conditions in other areas of the watershed, relative to the OL experiment (Figs. 6(c) and 6(d)).

The relative difference between the EnKF and OL experiments is also visualized by normalizing the trafficability risk diagnosed from the EnKF experiment by those diagnosed from the OL experiment. Figure 6(e) shows the probability of slow-go conditions diagnosed from the EnKF experiment normalized by the probability of slow-go conditions diagnosed from the OL experiment. Values of this ratio greater than unity indicate areas in the watershed where the EnKF experiment suggests higher trafficability risk than the OL experiment, while values less than unity suggest the contrary (Fig. 6(e)). Note that where the OL probability is zero and EnKF probability is non-zero, the ratio is plotted in red. This is consistent with locations where the EnKF probability is greater than the associated OL probability. In much of the eastern and southwestern part of the watershed, the risk of slow-go conditions suggested by the EnKF experiment is substantially higher than the corresponding risk diagnosed from the OL experiment (Fig. 6(e)). On the other hand, in the northwest, north central, and northeastern part of the watershed, the EnKF experiment suggests a substantially lower risk of slow-go conditions than the OL experiment (Fig. 6(e)). The corresponding visualization for the ratio of probability of no-go conditions for the EnKF experiment to that for the OL experiment is shown in Figure 6(f). Again, where the OL probability is zero and EnKF probability is non-zero, the ratio is plotted in red. In much of the watershed, the probability of no-go conditions is lower in the EnKF experiment than in the OL experiment (Fig. 6(f)). Again in the southwest portion of the watershed, however, the EnKF suggests higher probability of no-go conditions than the OL experiment.

4. Discussion

For the OSSE conducted in this study, the EnKF experiment was associated with substantially different probabilities of slow- and no-go conditions the corresponding probabilities of slow- and no-go conditions associated with the OL experiment. Specifically, for an analysis (EnKF update) that closely followed the occurrence of a large rain event, the EnKF framework suggested risks of encountering impaired trafficability conditions in parts of the watershed that were substantially above the risks diagnosed from the OL experiment.

This case study was designed as a synthetic experiment to demonstrate the potential use of anticipated microwave observations that are broadly consistent with the SMAP mission for military trafficability assessment. In particular, we use the EnKF as a mathematical framework to downscale synthetic L-band microwave radar observations with a spatial resolution of 3 km to spatial scales consistent with trafficability assessment (10s to 100s of m). The results suggest that assimilation of soil moisture data can improve model-based soil moisture estimates at scales useful for military trafficability assessment, even when the observations are of a significantly coarser spatial resolution than the model. In the discussion of [8], the authors provide a broader discussion of how the data assimilation system applied here to trafficability assessment could be enhanced to further increase realism or improve soil moisture estimation in advance of the launch of SMAP. Here, we focus more narrowly on how the data assimilation system might be better tailored to meet the needs of military trafficability assessment.

The IEM is best suited to sparsely vegetated or bare soil conditions [21]. Although volume scattering due to vegetation is likely low (particularly at L-band) in the desert environment considered in this cast study, in non-desert environments microwave volume scattering caused by water in vegetation canopies can be significant [45]. Vegetation also plays a significant role in the redistribution of moisture in the subsurface and particularly in the 0 to 40 cm horizon considered in this study. Future efforts will consider forested catchments where the role of vegetation in both moisture redistribution and microwave scattering is non-negligible. As previously mentioned a multiplicative error model is more appropriate to represent the speckle noise common to radar images than the Gaussian additive

NOTICE: This is the author's version of a work that was accepted for publication in *Journal of Terramechanics*. Changes resulting from the publishing process, such as peer review, editing, corrections, structural formatting, and other quality control mechanisms may not be reflected in this document. Changes may have been made to this work since it was submitted for publication. A definitive version was subsequently published in *Journal of Terramechanics*, Vol. 51, (2014). DOI: 10.1016/j.jterra.2013.11.004

white noise assumed in this study. In larger simulation domains, the difference between a multiplicative and additive error mode will be more pronounced, necessitating the use of the more appropriate multiplicative error model. We are also pursuing further data assimilation experiments to evaluate the anticipated hillslope-scale estimation errors for a range of noise levels and radar resolutions.

Ongoing effort also seeks to use the developed soil moisture data assimilation system within a more comprehensive trafficability assessment regime. This will require integration of additional landscape variables that are important when assessing the likelihood that a particular vehicle will encounter impaired mobility. A number of existing decision-making aids or experimental trafficability assessment frameworks could be applied for use with the soil moisture data assimilation system used here.

The Integrated Weather Effects Decision Aid (IWEDA), for example, is a software platform that ingests weather information from a variety of sources and, based on a suite of heuristic rules, provides maps of potential locations where military operations and weapons systems will be impaired by weather [46]. The weather data input to IWEDA go beyond soil moisture information and can include topography, forecast wind fields, cloud conditions, and air temperatures. More recently, the Army Remote Moisture System (ARMS) evolved from a tri-agency effort (US Department of Agriculture, USACE and NASA) to develop a platform capable of predicting soil moisture over large areas (up to 25,000 km^2) down to tactical scales (<100 m) [47]. The ARMS relies heavily upon simulation modeling, but also uses SAR imagery to constrain soil hydraulic parameters input to land surface hydrology models using the Parameter ESTimation (PEST) platform. Although not operational, the objective of ARMS is to provide a user-friendly tool to predict soil moisture at spatial scales appropriate for tactical mobility assessment at any location regardless of the paucity of data. Future work will investigate how a data assimilation system like the one applied here could be used to support more comprehensive assessment of weather impacts on military operations and weapons systems than the simple trafficability assessment index used in this study.

5. Conclusions

In this study, we applied an existing data assimilation system for soil moisture prediction at the hillslope scale to a relatively simple trafficability assessment exercise. An index of trafficability, RCI, was calculated from a series of empirical equations that require volumetric soil moisture information as input. This soil moisture information was obtained from either the outputs of a data assimilation state update (the EnKF experiment) or from an open loop (OL) experiment. Based on benchmark values of RCI for a particular vehicle (i.e., the VCI_1 and VCI_{50} values), the locations where impaired trafficability would be encountered could be mapped. Because the numerical experiments performed here were based on Monte Carlo simulation, an ensemble of these vehicle trafficability maps were produced and analyzed. Specifically, the ensemble of trafficability maps allowed for the assessment of the risk or probability of impaired trafficability conditions in the landscape. This probabilistic trafficability assessment allows us to communicate some measure of uncertainty in the predicted trafficability conditions.

Beyond military trafficability assessment, other applications requiring soil moisture information at these spatial scales could benefit from data assimilation approaches using microwave observations from platforms like SMAP and SMOS. The use of ensemble-based simulation in these applications allows for the communication of not only a spatial map of occurrence of some outcome, but also the associated risk of that outcome. Some applications that have a need for soil moisture information at hillslopes scales include soil water deficit for irrigation scheduling and slope-stability formulations for landslide hazard assessment.

Acknowledgements

This work was supported by U.S. Army RDECOM ARL Army Research Office under grants W911NF-04-1-0119, W911NF-09-1-0534, W911NF-11-1-0310, W911NF-12-1-0095, NASA grants NNG05GA17G, NNX10AG84G, and NNX11AQ33G, and the MIT Martin Family Society of Fellows for Sustainability.

NOTICE: This is the author's version of a work that was accepted for publication in *Journal of Terramechanics*. Changes resulting from the publishing process, such as peer review, editing, corrections, structural formatting, and other quality control mechanisms may not be reflected in this document. Changes may have been made to this work since it was submitted for publication. A definitive version was subsequently published in *Journal of Terramechanics*, Vol. 51, (2014). DOI: 10.1016/j.jterra.2013.11.004

References

[1] GCOS, Implementation plan for the Global Observing System for climate in support of the UNFCCC-2010 update, report, World Meteorological Organization, Geneva Switzerland, 2010.

[2] M. Nolan and D. R. Fatland, New DEMs may stimulate significant advancements in remote sensing of soil moisture, Eos Transactions of the AGU, 84 (2003), 233–237, doi:10.1029/2003EO250001.

[3] V. R. N. Pauwels, R. Hoeben, N. E. C. Verhoest, and F. P. De Troch, The importance of the spatial patterns of remotely sensed soil moisture in the improvement of discharge predictions for small-scale basins through data assimilation, Journal of Hydrology, 251 (2001), 88-102, doi:10.1016/S0022-1694(01)00440-1.

[4] R. H. Reichle, D. B. McLaughlin, and D. Entekhabi, Hydrologic data assimilation with the Ensemble Kalman filter, Monthly Weather Review, 130 (2002), 103-114.

[5] R. H. Reichle, D. Entekhabi, and D. B. McLaughlin, Downscaling of radiobrightness measurements for soil moisture estimation: A four-dimensional variational data assimilation approach, Water Resources Research, 37 (2001), 2353-2364, doi:10.1029/2001WR000475.

[6] J. F. Galantowicz, D. Entekhabi, and E. G. Njoku, Tests of sequential data assimilation for retrieving profile soil moisture and temperature from observed L-band radiobrightness, IEEE Transactions on Geoscience and Remote Sensing, 37 (1999), 1860-1870.

[7] E. Altese, O. Bolognani, M. Mancini, and P. A. Troch, Retrieving soil moisture over bare soil from ERS 1 synthetic aperture radar data: Sensitivity analysis based on a theoretical surface scattering model and field data, Water Resources Research, 32 (1996), 653-661.

[8] A. N. Flores, R. L. Bras, and D. Entekhabi, Hydrologic data assimilation with a hillslope-scale resolving model and L-band radar observations: Synthetic experiments with the ensemble Kalman filter, Water Resources Research, 48 (2012), W08509, doi:10.1029/2011WR011500.

[9] W. L. Crosson, C. A. Laymon, R. Inguva, and M. P. Schamschula, Assimilating remote sensing data in a surface flux–soil moisture model, Hydrological Processes, 16 (2002), 1645-1662, doi: 10.1002/hyp.1051.

[10] G. Evensen, Sequential data assimilation with a nonlinear quasi-geostrophic model using Monte Carlo methods to forecast error statistics, Journal of Geophysical Research, 99 (1994), 10,143-10,162.

[11] G. Evensen, Sampling strategies and square root analysis schemes for the EnKF, Ocean Dynamics, 54 (2004), 539-560.

[12] H. Moradkhani, C. M.DeChant, and S.Sorooshian, Evolution of ensemble data assimilation for uncertainty quantification using the particle filter-Markov chain Monte Carlo method, Water Resources Research, 48 (2012), W12520, doi:10.1029/2012WR012144.

[13] S. Dunne and D. Entekhabi, Land surface state and flux estimation using the ensemble Kalman smoother during the Southern Great Plains 1997 field experiment, Water Resources Research, 42 (2006), W01407, doi:10.1029/2005WR004334.

[14] W. Ni-Meister, Recent advances on soil moisture data assimilation, Physical Geography, 29 (2008), 19-37.

[15] R. Jones, D. Horner, P. Sullivan, and R. Ahlvin, A methodology for quantitatively assessing vehicular rutting on terrains, Journal of Terramechanics, 42 (2005), 245-257.

[16] J. D. Priddy and W. E. Willoughby, Clarification of vehicle cone index with reference to mean maximum pressure, Journal of Terramechanics, 43 (2006), 85-96.

[17] I. C. Schmid, Interaction of vehicle and terrain results from 10 years research at IKK, Journal of Terramechanics, 32 (1995), 3-26.

[18] A. N. Flores, D. Entekhabi, and R. L. Bras, Reproducibility of soil moisture ensembles when representing soil parameter uncertainty and correlation using a Latin Hypercube-based approach, Water Resources Research, 46 (2010), doi:10.1029/2009WR008155.

[19] V. Y. Ivanov, R. L. Bras, and D. C. Curtis, A weather generator for hydrological, ecological, and agricultural applications, Water Resources Research, 43 (2007), doi: 10.1029/2006WR005364.

[20] D. Entekhabi, E. G. Njoku, P. E. O'Neill, K. H. Kellogg, W. T. Crow, W. N. Edelstein, J. K. Entin, S. D. Goodman, T. J. Jackson, J. Johnson, J. Kimball, J. R. Piepmeier, R. D. Koster, N. Martin, K. C. McDonald, M. Moghaddam, S. Moran, R. Reichle, J. C. Shi, M. W. Spencer, S. W. Thurman, L. Tsang, and J. Van Zyl, The Soil Moisture Active Passive (SMAP) Mission, Proceedings of the IEEE, 98 (2010), 704-716.

[21] A. K. Fung, Z. Li, and K. S. Chen, Backscattering from a randomly rough dielectric surface, IEEE Transactions on Geoscience and Remote Sensing, 30 (1992), 356–369.

[22] A. K. Fung, Microwave Scattering and Emission Models and Their Applications, Artech House, Boston, 1994.

NOTICE: This is the author's version of a work that was accepted for publication in *Journal of Terramechanics*. Changes resulting from the publishing process, such as peer review, editing, corrections, structural formatting, and other quality control mechanisms may not be reflected in this document. Changes may have been made to this work since it was submitted for publication. A definitive version was subsequently published in *Journal of Terramechanics*, Vol. 51, (2014). DOI: 10.1016/j.jterra.2013.11.004

[23] R. Hoeben and P. A. Troch, Assimilation of active microwave observation data for soil moisture profile estimation, Water Resources Research, 36 (2000), 2805-2819.

[24] T. J. Smith, J. P. McNamara, A. N. Flores, M. M. Gribb, P. S. Aishlin, and S. G. Benner, Small soil storage capacity constrains upland benefits of winter snowpack, Hydrological Processes, 25 (2011), 3858-3865, doi:10.1002/hyp.8340.

[25] C. Matzler and A. Standley, Technical note: Relief effects for passive microwave remote sensing, International Journal of Remote Sensing, 21 (2000), 2403–2412.

[26] A. N. Flores, V. Y. Ivanov, D. Entekhabi, and R. L. Bras, Impacts of hillslope-scale organization in topography, soil moisture, soil temperature, and vegetation on modeling surface microwave radiation emission, IEEE Transactions on Geoscience and Remote Sensing, 47 (2009), 2557-2571.

[27] V. Y. Ivanov, E. R. Vivoni, R.L. Bras, and D. Entekhabi, Preserving high-resolution surface and rainfall data in operational-scale basin hydrology: a fully-distributed physically-based approach, Journal of Hydrology, 298 (2004), 80-111.

[28] V. Y. Ivanov, E. R. Vivoni, R. L. Bras, and D. Entekhabi, Catchment hydrologic response with a fully distributed triangulated irregular network model, Water Resources Research, 40 (2004), W11102, doi:10.1029/2004WR003218.

[29] V. Y. Ivanov, R. L. Bras, and E. R. Vivoni, Vegetation-hydrology dynamics in complex terrain of semi-arid areas: 1. A mechanistic approach to modeling dynamic feedbacks, Water Resources Research, 44 (2008), doi:10.1029/2006WR005588.

[30] V. Y. Ivanov, R. L. Bras, and E. R. Vivoni, Vegetation-hydrology dynamics in complex terrain of semi-arid areas: 2. Energy-water controls of vegetation spatio-temporal dynamics and topographic niches of favorability, Water Resources Research, 44 (2008), doi:10.1029/2006WR005595.

[31] T. G. Farr et al., The Shuttle Radar Topography Mission, Review of Geophysics, 45 (2007), RG2004, doi:10.1029/2005RG000183.

[32] G. C. Topp, J. L. Davis, A. P. Annan, Electromagnetic determination of soil water content: Measurements in coaxial transmission lines, Water Resources Research, 16 (1980), 574-582.

[33] Y. H. Kerr, P. Waldteufel, J.-P. Wigneron, J.-M. Martinuzzi, J. Font, and M. Berger, Soil moisture retrieval from space: The Soil Moisture and Ocean Salinity (SMOS) mission, IEEE Transactions on Geoscience and Remote Sensing, 39 (2001), 1729-1735.

[34] Y. Kerr, F. Secherre, J. Lastenet, and J.-P. Wigneron, SMOS: Analysis of perturbing effects over land surfaces, In Proc. IGARSS, 2 (2003), 908-910.

[35] G. Evensen, The ensemble Kalman Filter: theoretical formulation and practical implementation, Ocean Dynamics, 53 (2003), 343-367.

[36] M. S. Moran, W. E. Emmerich, D. C. Goodrich, P. Heilman, C. D. Holifield-Collins, T. O. Keefer, M. A. Nearing, et al., Preface to the special section on Fifty Years of Research and Data Collection: U. S. Department of Agriculture Walnut Gulch Experimental Watershed, Water Resources Research, 44 (2008), W05S01, doi:10.1029/2007WR006083.

[37] S. Islam, D. Entekhabi, R. L. Bras, and I. Rodriguez-Iturbe, Parameter estimation and sensitivity analysis for the modified Bartlett-Lewis rectangular pulses model of rainfall, Journal of Geophysical Research, 95 (1990), 2093-2100.

[38] L. Ferraris, S. Gabellani, N. Rebora, and A. Provenzale, A comparison of stochastic models for spatial rainfall downscaling, Water Resources Research, 39 (2003), doi:10.1029/2003WR002504.

[39] F. T. Ulaby, P. C. Dubois, and J. Van Zyl, Radar mapping of surface soil moisture. Journal of Hydrology, 184 (1996), 57-84.

[40] M. P. Meyer, I. R. Ehrlich, D. Sloss, N. R. Murphy, Jr., R. D. Wismer, and T.Czako, International society for terrain-vehicle systems standards, Journal of Terramechanics, 14 (1977), 153–182.

[41] S. A. Shoop, Terrain Characterization for Trafficability, U.S. Army Corps of Engineers, Cold Regions Research and Engineering Laboratory, CRREL Report 93-6, 1993.

[42] J. J. Daigle, W. H. Hudnall, W. J. Gabriel, E. Mersiovsky, and R. D. Nielson, The National Soil Information System (NASIS): Designing soil interpretation classes for military land-use predictions, Journal of Terramechanics, 42 (2005), 305–320.

[43] P. M. Sullivan, C. D. Bullock, N. A. Renfroe, M. R. Albert, G. G. Koening, L. Peck, and K. O'Neill, Soil moisture strength prediction model version II (SMSP II), U.S. Army Corps of Engineers Waterways Experiment Station, Vicskburg, MS, Technical Report GL-97-15, 1997.

[44] US Army, Planning and design of roads, airfields, and heliports in the theatre of operations–road design, Department of the Army, Washington, DC, US Army FM 5-430-00-1, 1994.

NOTICE: This is the author's version of a work that was accepted for publication in *Journal of Terramechanics*. Changes resulting from the publishing process, such as peer review, editing, corrections, structural formatting, and other quality control mechanisms may not be reflected in this document. Changes may have been made to this work since it was submitted for publication. A definitive version was subsequently published in *Journal of Terramechanics*, Vol. 51, (2014). DOI: 10.1016/j.jterra.2013.11.004

[45] R. Bindlish and A. P. Barros, Parameterization of vegetation backscatter in radar-based, soil moisture estimation, Remote Sensing of Environment, 76 (2001), 130-137, 10.1016/S0034-4257(00)00200-5.

[46] C. H. Chesley and V. P. Grocki, Verification and Validation of Current IWEDA Rules, No. STC-TR-3157, Science and Technology Corp., Hampton, VA, 1997.

[47] M. Tischler, M. Garcia, C. Peters-Lidard, M. S. Moran, S. Miller, D. Thoma, and J. Geiger, A GIS framework for surface-layer soil moisture estimation combining satellite radar measurements and land surface modeling with soil physical property estimation, Environmental Modelling and Software, 22 (2007), 891-898.

NOTICE: This is the author's version of a work that was accepted for publication in *Journal of Terramechanics*. Changes resulting from the publishing process, such as peer review, editing, corrections, structural formatting, and other quality control mechanisms may not be reflected in this document. Changes may have been made to this work since it was submitted for publication. A definitive version was subsequently published in *Journal of Terramechanics*, Vol. 51, (2014). DOI: 10.1016/j.jterra.2013.11.004

Tables

Table 1: Properties of tRIBS-VEGGIE mesh and EnKF experiment

Property	Value
Watershed area [km^2]	148
Number of pixels [-]	19,447
Effective resolution [m]	87.2
Number of soil layers [-]	10
Number of soil textures [-]	27
Minimum/maximum/mean elevation [m]	1222/1933/1420
State vector dimension [-]	194,470
Number of observations [-]	60
Number of EnKF replicates [-]	256
Number of analysis periods [-]	9

Table 2: Coefficients for trafficability index-soil moisture relationship

Soil textural class	a	b
Silty sand	12.524	-2.955
Clayey sand	15.506	-3.530
Clay	11.936	-2.471
Silt	14.236	-3.137
Clay of high plasticity	13.686	-2.705
Silt of high plasticity	23.641	-5.191
Organic silt, organic clay	17.399	-3.584
Organic clay, organic silt	12.189	-1.924

Table 3: Summary of ensemble mean soil moisture, RMSE, and percent reduction in RMSE

	OL Experiment	EnKF Experiment	
Ensemble mean soil moisture	0.206	0.204	**Average % Reduction RMSE**
Ensemble RMSE soil moisture	0.105	0.064	35.7

NOTICE: This is the author's version of a work that was accepted for publication in *Journal of Terramechanics*. Changes resulting from the publishing process, such as peer review, editing, corrections, structural formatting, and other quality control mechanisms may not be reflected in this document. Changes may have been made to this work since it was submitted for publication. A definitive version was subsequently published in *Journal of Terramechanics*, Vol. 51, (2014). DOI: 10.1016/j.jterra.2013.11.004

Figures

Figure Captions

Figure 1: A data assimilation-enhanced trafficability assessment workflow depicting the numerical experiments outlined in this study. Tools and models are shown in light gray, while outputs of the trafficability assessment are shaded in dark grey.

Figure 2: A conceptual diagram of the EnKF algorithm. Initial soil moisture estimates are propagated forward in time to produce a forecast when an observation is available. This soil moisture forecast is input to the forward geophysical model to produce a forecast of the observations. These are then used together with the actual observations, taking into account their uncertainty, to update the forecast soil moisture. This updated soil moisture ensemble – the analysis – is then used to reinitialize the hydrologic model.

Figure 3: The distribution of (a) elevation, (b) slope gradient, (c) soil textural classes, and (d) total precipitation during the course of the experiment for WGEW, which is located in (e) southwestern Arizona, USA. The reader is referred to Flores et al. [2012] for a table of the soil textural classes, which is not repeated here for brevity.

Figure 4: Ensemble mean soil moisture in the top 40 cm of the soil column is shown for the (a) true, (b) OL and (c) EnKF experiments. Corresponding root mean squared error (RMSE) values relative to the synthetic true soil moisture are shown for the (d) OL and (e) EnKF experiments.

Figure 5: Ensemble mean RCI values based on soil moisture in the top 40 cm of the soil column are shown for the (a) synthetic true, (b) OL and (c) EnKF experiments. Corresponding RMSE values relative to the corresponding RCI values based on the synthetic true soil moisture are shown for the (d) OL and (e) EnKF experiments.

Figure 6: Probability of slow-go conditions diagnosed from the soil moisture ensembles is shown for the (a) OL and (b) EnKF experiments. Probability of no-go conditions is shown for the (c) OL and (d) EnKF experiments. In (e) the ratio of probability of slow go conditions diagnosed from the EnKF to the OL experiment is shown. In (f) the corresponding ratio for no-go conditions is shown.

NOTICE: This is the author's version of a work that was accepted for publication in *Journal of Terramechanics*. Changes resulting from the publishing process, such as peer review, editing, corrections, structural formatting, and other quality control mechanisms may not be reflected in this document. Changes may have been made to this work since it was submitted for publication. A definitive version was subsequently published in *Journal of Terramechanics*, Vol. 51, (2014). DOI: 10.1016/j.jterra.2013.11.004

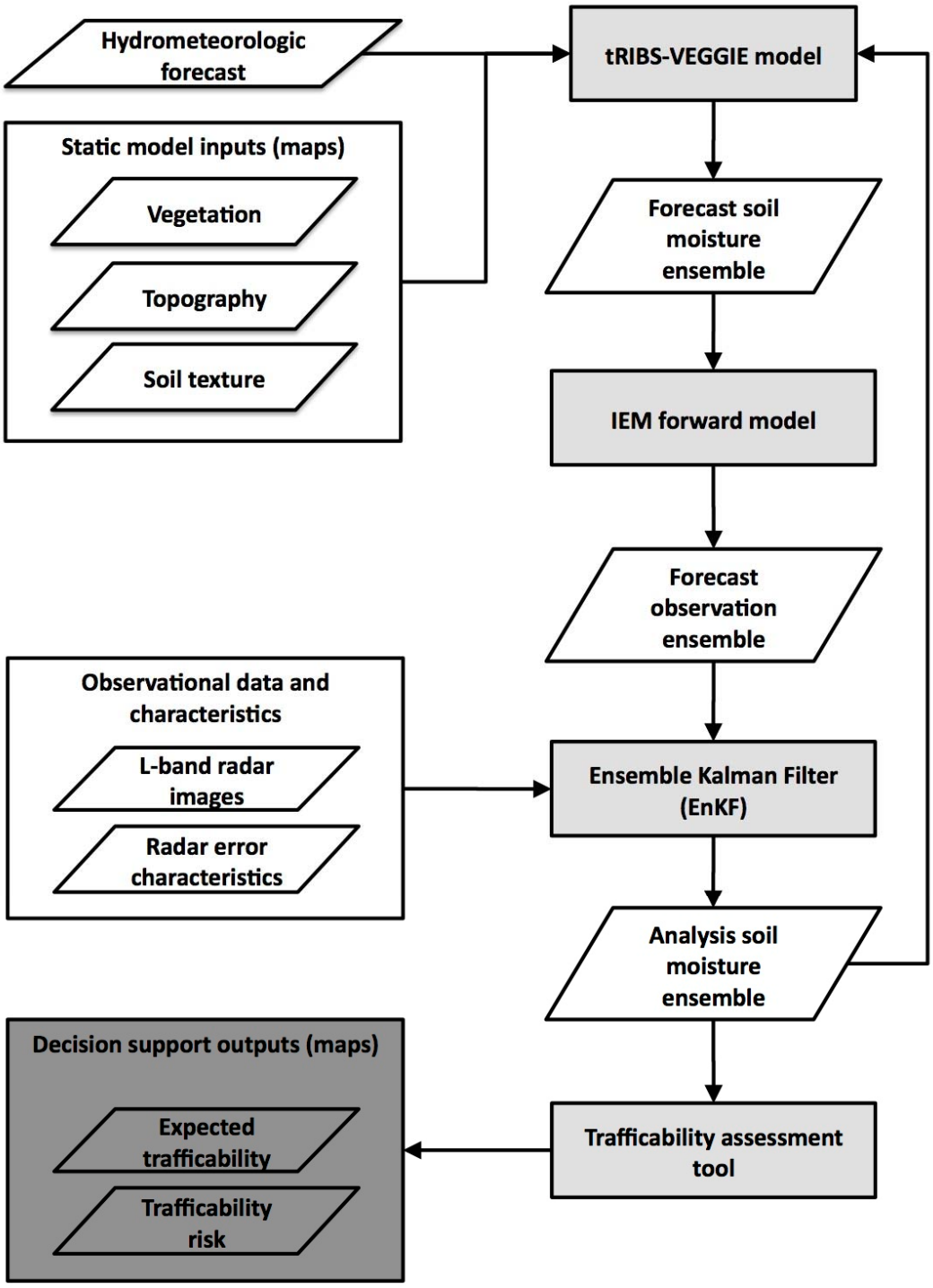

Figure 1: A data assimilation-enhanced trafficability assessment workflow depicting the numerical experiments outlined in this study. Tools and models are shown in light gray, while outputs of the trafficability assessment are shaded in dark grey.

NOTICE: This is the author's version of a work that was accepted for publication in *Journal of Terramechanics*. Changes resulting from the publishing process, such as peer review, editing, corrections, structural formatting, and other quality control mechanisms may not be reflected in this document. Changes may have been made to this work since it was submitted for publication. A definitive version was subsequently published in *Journal of Terramechanics*, Vol. 51, (2014). DOI: 10.1016/j.jterra.2013.11.004

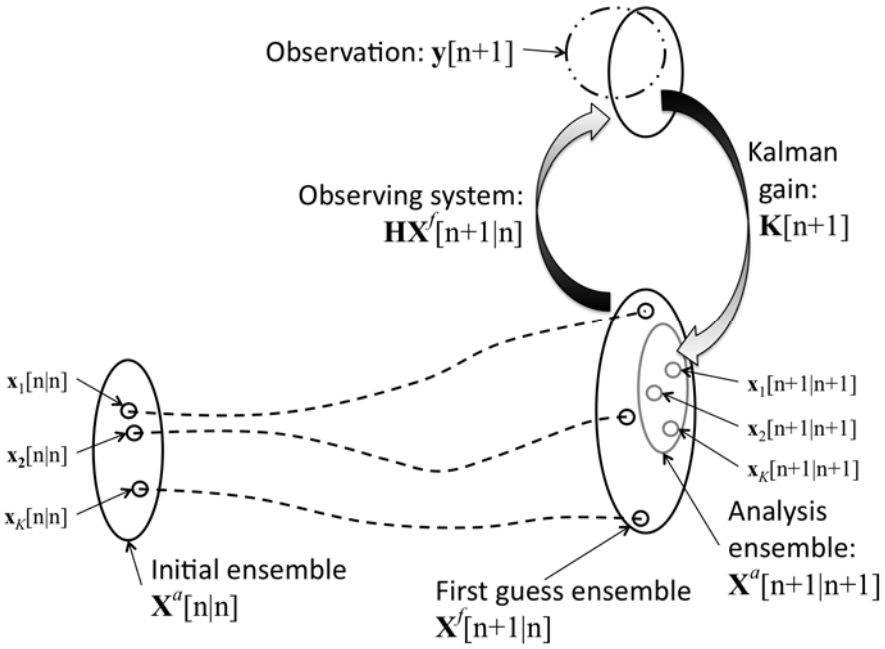

Figure 2: A conceptual diagram of the EnKF algorithm. Initial soil moisture estimates are propagated forward in time to produce a forecast when an observation is available. This soil moisture forecast is input to the forward geophysical model to produce a forecast of the observations. These are then used together with the actual observations, taking into account their uncertainty, to update the forecast soil moisture. This updated soil moisture ensemble – the analysis – is then used to reinitialize the hydrologic model.

NOTICE: This is the author's version of a work that was accepted for publication in *Journal of Terramechanics*. Changes resulting from the publishing process, such as peer review, editing, corrections, structural formatting, and other quality control mechanisms may not be reflected in this document. Changes may have been made to this work since it was submitted for publication. A definitive version was subsequently published in *Journal of Terramechanics*, Vol. 51, (2014). DOI: 10.1016/j.jterra.2013.11.004

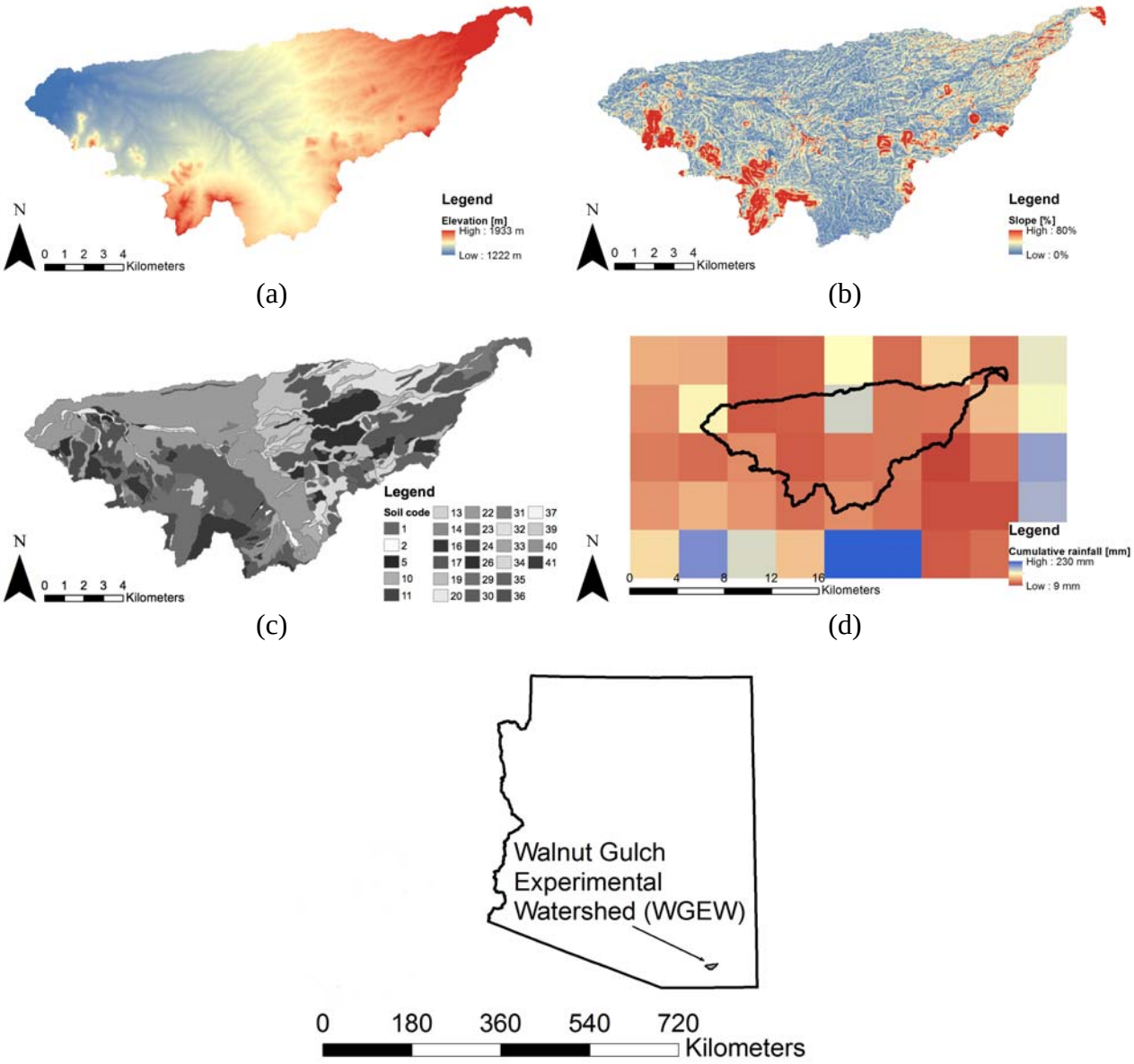

Figure 3: The distribution of (a) elevation, (b) slope gradient, (c) soil textural classes, and (d) total precipitation during the course of the experiment for WGEW, which is located in (e) southwestern Arizona, USA. The reader is referred to Flores et al. [2012] for a table of the soil textural classes, which is not repeated here for brevity.

NOTICE: This is the author's version of a work that was accepted for publication in *Journal of Terramechanics*. Changes resulting from the publishing process, such as peer review, editing, corrections, structural formatting, and other quality control mechanisms may not be reflected in this document. Changes may have been made to this work since it was submitted for publication. A definitive version was subsequently published in *Journal of Terramechanics*, Vol. 51, (2014). DOI: 10.1016/j.jterra.2013.11.004

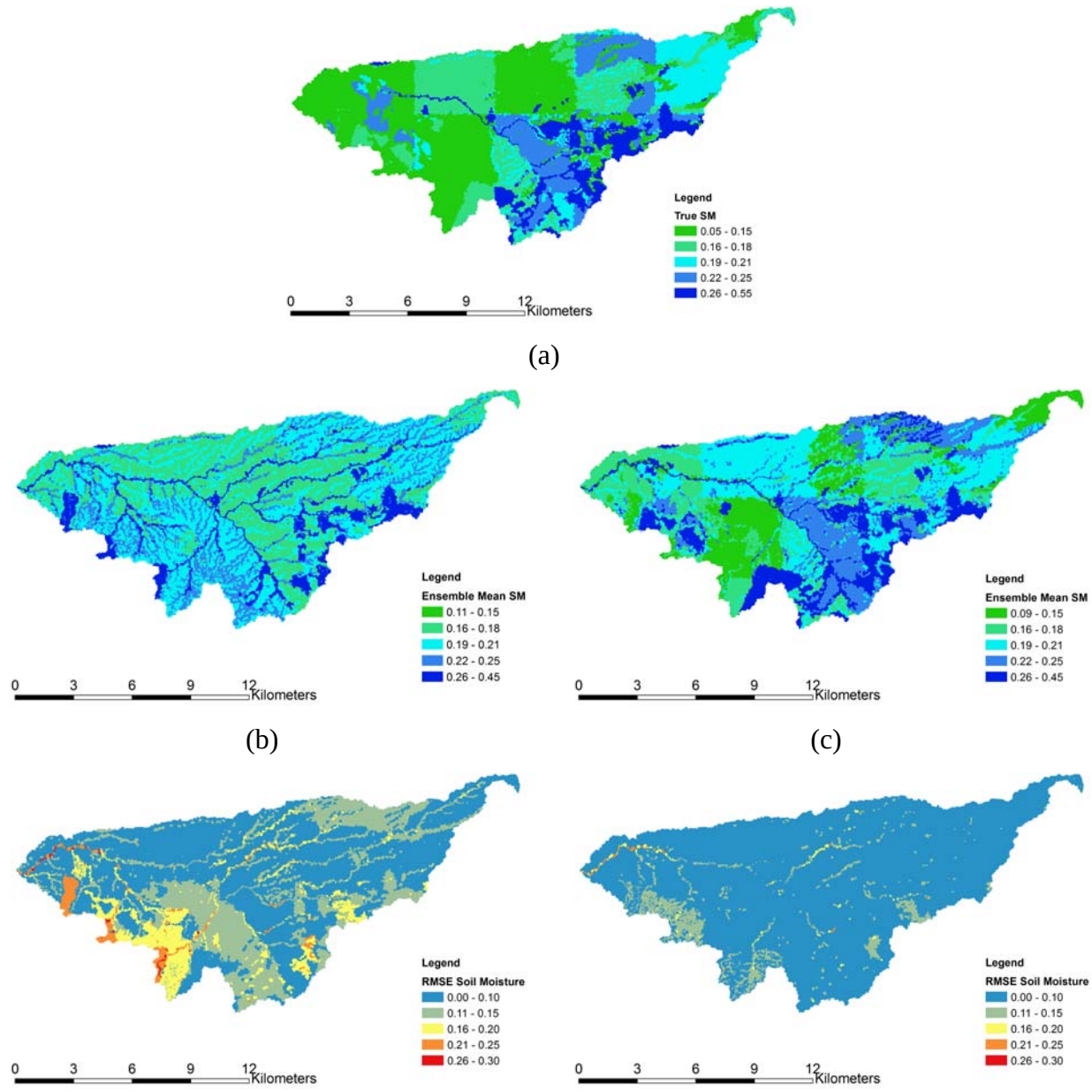

Figure 4: Ensemble mean soil moisture in the top 40 cm of the soil column is shown for the (a) true, (b) OL and (c) EnKF experiments. Corresponding root mean squared error (RMSE) values relative to the synthetic true soil moisture are shown for the (d) OL and (e) EnKF experiments.

NOTICE: This is the author's version of a work that was accepted for publication in *Journal of Terramechanics*. Changes resulting from the publishing process, such as peer review, editing, corrections, structural formatting, and other quality control mechanisms may not be reflected in this document. Changes may have been made to this work since it was submitted for publication. A definitive version was subsequently published in *Journal of Terramechanics*, Vol. 51, (2014). DOI: 10.1016/j.jterra.2013.11.004

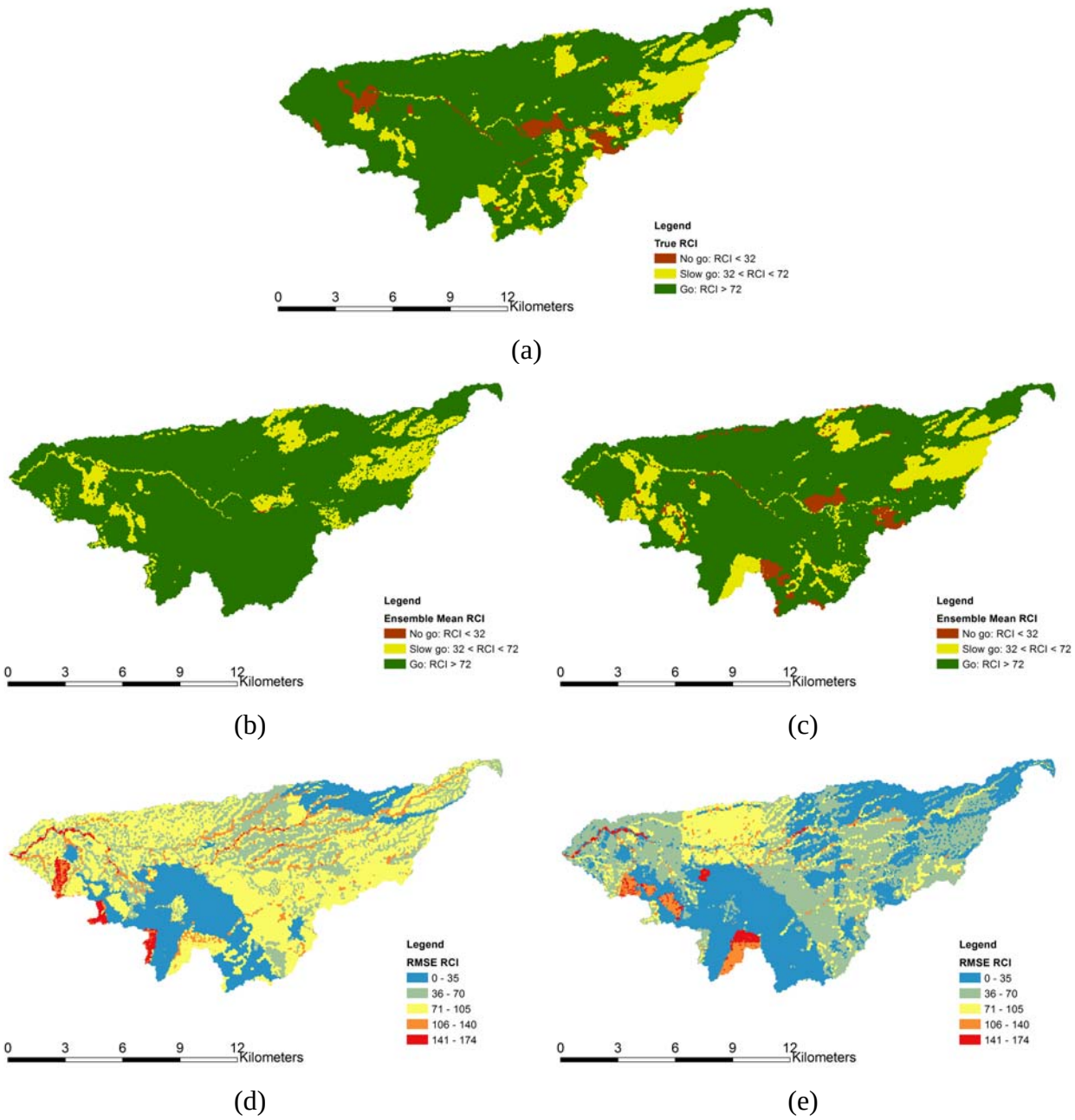

Figure 5: Ensemble mean RCI values based on soil moisture in the top 40 cm of the soil column are shown for the (a) synthetic true, (b) OL and (c) EnKF experiments. Corresponding RMSE values relative to the corresponding RCI values based on the synthetic true soil moisture are shown for the (d) OL and (e) EnKF experiments.

NOTICE: This is the author's version of a work that was accepted for publication in *Journal of Terramechanics*. Changes resulting from the publishing process, such as peer review, editing, corrections, structural formatting, and other quality control mechanisms may not be reflected in this document. Changes may have been made to this work since it was submitted for publication. A definitive version was subsequently published in *Journal of Terramechanics*, Vol. 51, (2014). DOI: 10.1016/j.jterra.2013.11.004

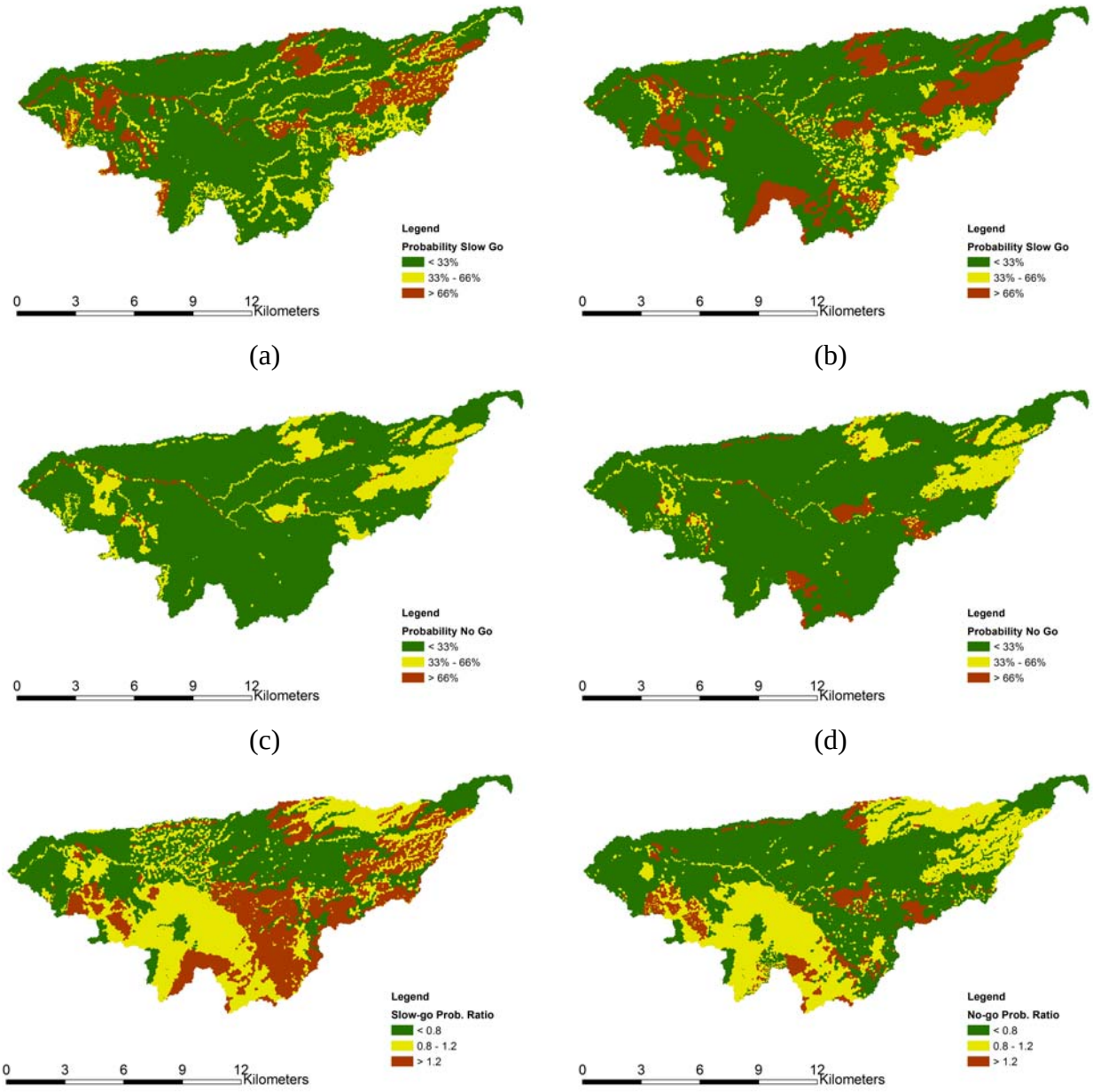

Figure 6: Probability of slow-go conditions diagnosed from the soil moisture ensembles is shown for the (a) OL and (b) EnKF experiments. Probability of no-go conditions is shown for the (c) OL and (d) EnKF experiments. In (e) the ratio of probability of slow go conditions diagnosed from the EnKF to the OL experiment is shown. In (f) the corresponding ratio for no-go conditions is shown.